J Appl Electrochem (2009) 39:2291–2295
DOI 10.1007/s10800-009-9806-5

ORIGINAL PAPER

Using EIS for diagnosis of dye-sensitized solar cells performance

M. Liberatore · F. Decker · L. Burtone · V. Zardetto · T. M. Brown · A. Reale · A. Di Carlo

Received: 7 October 2008 / Accepted: 21 January 2009 / Published online: 19 February 2009

Abstract During the last decade interest in dye-sensitized solar cells (DSC) has grown enormously. Electrical impedance spectroscopy (EIS) is an electrochemical technique commonly used for investigation of charge carrier dynamics in these photovoltaic devices. We used EIS for characterization of our DSC; moreover, symmetric cells with counter–counter or photo–photo electrodes were realized and measured in order to simplify impedance cell analysis by separating the contribution of counter and photoelectrode, respectively. In particular, we provided very accurate illumination of the photoelectrode symmetric cell, aiming to approach the experimental conditions of a complete cell. By fitting of experimental data, we obtained values for the charge transfer resistance at the counter-electrode and the electron percolation time at the photoelectrode. Moreover, the simulation of a whole cell, combining the data from the fitting procedures above, was in good agreement with experimental data.

Keywords Dye-sensitized solar cells · Photoanode · Impedance · Symmetric cell

M. Liberatore (✉) · L. Burtone · V. Zardetto · T. M. Brown · A. Reale · A. Di Carlo
Center for Hybrid Organic Solar Energy (CHOSE), Department of Electronic Engineering, University of Rome "Tor Vergata", via del Politecnico 1, 00133 Rome, Italy
e-mail: liberatore@ing.uniroma2.it

F. Decker
Chemistry Department, University of Rome "La Sapienza", piazzale A. Moro 5, 00185 Rome, Italy

1 Introduction

Dye-sensitized solar cells (DSC) [1] are modern electrochemical devices for conversion of solar energy, consisting of three main components: the dye-sensitized nanocrystalline TiO_2 layer on a transparent conductive oxide (the photoelectrode), the platinized transparent conductive oxide counterelectrode (Pt/TCO; usually the TCO is a F-doped tin dioxide layer on glass, or FTO), and an organic electrolyte containing a redox couple and additives. It is commonly accepted that the main factors limiting the solar-to-electrical energy conversion efficiency are recombination at the photoelectrode (the back reaction), insufficient catalytic activity of the Pt/FTO for the redox couple reduction, and the overall cell series resistance attributable in part to the slow ion transport. To study the latter, current–voltage characteristics with different cell geometries have been analyzed [2, 3]. Regarding the catalytic activity of the Pt/FTO counterelectrode, Hauch and Georg [4] measured the charge-transfer resistance (R_{ct}) with electrochemical impedance spectroscopy (EIS) using a symmetric cell with two identical Pt/TCO electrodes. This approach has the advantage of isolating the performance of the counterelectrode alone, allowing, through data analysis with a simple equivalent-circuit model, the evaluation of R_{ct}. Several other authors [4–8] have discussed the charge-transfer reaction mechanism and the transfer coefficient of the iodide/triiodide redox couple at Pt/FTO, but their results are not in agreement with each other. The reaction mechanism at the photoelectrode has been studied by many researchers using a variety of electrochemical and optoelectronic techniques, for instance, intensity-modulated photovoltage spectroscopy (IMVS), intensity-modulated photocurrent spectroscopy (IMPS) [9–11], and transient absorption spectroscopy (TAS) [12, 13], pointing out that the time constant for electron

injection from the photoexcited dye orbital to the TiO_2 conduction band is ultrafast (in the pico/femtosecond domain) whereas the time constant for electron percolation through the mesoporous TiO_2 is on the order of a few milliseconds. Except for the ultrafast phenomena, EIS has been demonstrated to be a powerful tool for analysis of physicochemical processes occurring at both counter and photoelectrode; sometimes, especially when testing new materials for electrode production, accurate analysis of whole cell impedance is not possible, because of insufficiently separated time constants for cathodic and anodic phenomena. In this case, it is appropriate to use the mentioned approach of the symmetric cell. In this paper, first encouraging results are shown for the extension of the symmetric cell approach to the photoelectrode; by using this method, the influence of counter and photoelectrode on the complete cell performance was calculated separately. Moreover, the characteristic impedance of the complete cell was simulated using extrapolated parameters from the symmetric cells; the simulation showed good agreement with measured data. In conclusion, we show that the measurement of two symmetric cells (made of counter–counter or photo–photo electrodes) allows the prediction of the complete cell behavior.

2 Experimental

2.1 Cell preparation

Dye-sensitized photoelectrodes were prepared by deposition on FTO-coated glass of a slurry paste containing P25® Degussa titanium oxide powders, via Doctor Blade® technique. After annealing process at 450 °C for 30 min, we obtained a mesoporous Titania film whose thickness was 6 μm, as measured by Dektak 150® profilometer. Then, the films have been dipped for 14 h in an ethanolic 0.05 M solution of *cis*-bis(isothiocyanato)bis(2,2′-bipyridyl-4,4′-dicarboxylato)-ruthenium(II)bis-tetrabutylammonium, also known as N719. After this stage, they were rinsed in pure ethanol and dried using a nitrogen flux. The platinized electrodes were prepared by annealing at 400 °C for 5 min FTO-coated glasses previously sprayed with Platisol® solution. Finally photo and counterelectrodes were assembled together in three different cell configurations: photo–counter (termed also "plain cell"), counter–counter and photo–photo (both termed "symmetric cells"). About 60-μm-thick Surlyn® polymer film was used as both spacer and sealant. A thin layer of electrolyte Iodolyte R150® was introduced into the cell via a predrilled hole, using the vacuum backfilling technique. Finally, the hole was hermetically sealed with a small glass patch as well as Surlyn® film. The active area for all the samples was 0.25 cm^2.

2.2 Electrical measurements

For the plain cell, efficiency, open-circuit voltage, short-circuit current, and fill factor were calculated from the current–voltage characteristic curve, measured with an AUTOLAB PGSTAT12® potentiostat/galvanostat, under 1,000 W m^{-2} illumination provided by a halogen lamp equipped with an optical fiber in order to focus the light beam on the active area. Using a frequency response analyzer module integrated with the Ecochemie PGSTAT12, EIS measurements were performed on plain and symmetric cells. In particular, the plain cells were illuminated from the photoelectrode side, and the impedance spectra were taken at open-circuit potential condition; the counter–counter symmetric cells were measured in the dark at open-circuit potential (0 V); while the photo–photo symmetric cells were measured under illumination from both sides by an halogen lamp equipped with two distinct optical fibers, positioned in such way as to yield a cell voltage of 0 V. In the EIS experiments, the perturbation amplitude was 10^{-2} V and the frequency range was between 10^5 and 10^{-1} Hz.

2.3 Fit and simulation

Impedance data were plotted on a Nyquist diagram and the fit and simulation processes were achieved using ZSimpWin 3.22d® software. We underline that many equivalent circuits have been proposed in the literature to model dye-sensitized solar cells [14–18]. Both distributed and concentrated parameters circuits can be used, but we chose the latter because it is generally easier to find a coherent correlation between the parameters and physical phenomena. In this work, diffusion of ions inside the solution has not been fitted because the low-frequency measurements have too large oscillations to be reliable; indeed there is no diffusion element inside the equivalent circuit used. Figure 4 shows the equivalent circuit used for fitting a complete cell; it is composed of the series of two Randles-type circuits and a further series resistance. Each circuit characterized one electrode interface: TiO_2/dye/electrolyte and electrolyte/Pt/TCO, respectively. We specify that the introduction of a constant phase element (CPE) instead of a capacitance has been done because of the elevated porosity of interfaces. In the case of symmetric cells we assume identical reactions at the electrodes, therefore the above-mentioned circuit can be simplified according to Kirchhoff's laws to a single Randles-type circuit plus a series resistance.

3 Results and discussion

In Fig. 1 the current–voltage curve and main cell parameters of the plain cell under 1,000 Wm^{-2} illumination are

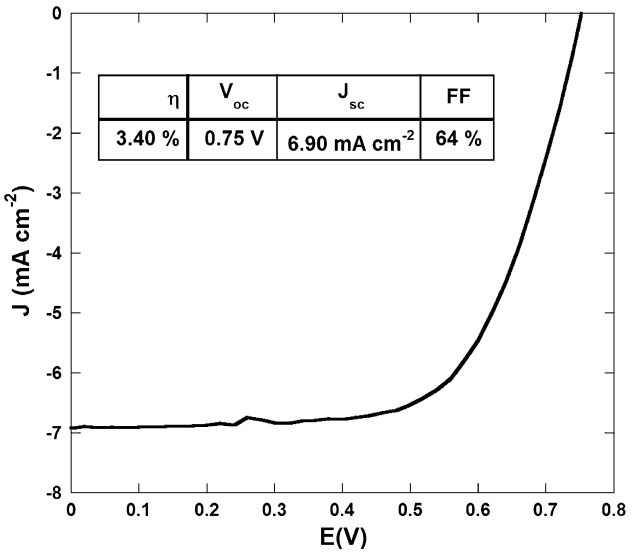

Fig. 1 Measured *I–V* curve of a plain cell under illumination of 1,000 Wm^{-2}. The main parameters values are summarized in Table 1

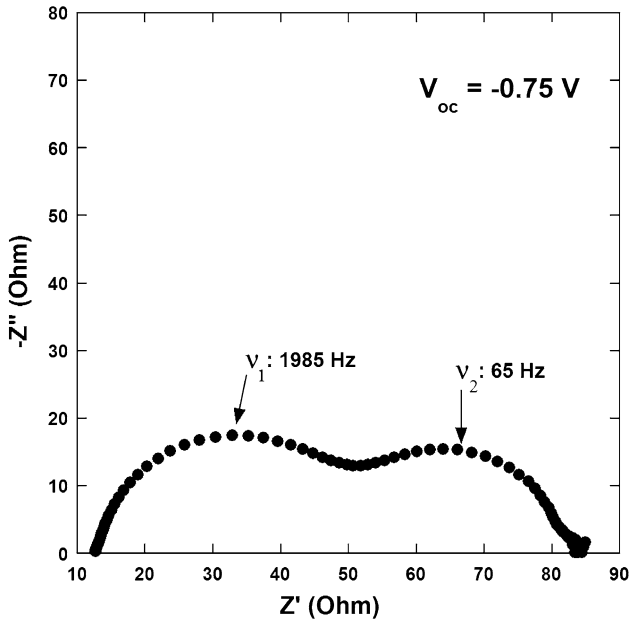

Fig. 2 Nyquist plot of EIS spectra measured between 10^5 and 10^{-1} Hz on a plain cell at $V_{OC} = -0.75$ V under illumination of 1,000 Wm^{-2}. The two characteristic frequencies of the main semicircles are marked

shown. The open-circuit voltage (V_{OC}) is given by the potential difference between the TiO_2 conduction band edge and the electrochemical potential of the redox couple in the electrolyte [19]. The short-circuit current (I_{sc}) is the maximum current value achieved when the cell is short-circuited. The fill factor (FF, the ratio between the maximum cell output power and the product $V_{oc} \times I_{sc}$) and energy conversion efficiency (η) with respect to incident light were measured and are slightly lower than those reported in literature for similar systems [20]. Therefore, EIS analysis was necessary in order to determine the causes of this performances loss. Thus, in Fig. 2, the impedance spectrum of plain cell in open-circuit condition is shown. We can identify two partially overlapped semicircles: a first one with characteristic $\nu_1 = 1{,}985$ Hz related to the charge transfer at the Pt/TCO-electrolyte interface [14] and a second one with characteristic $\nu_2 = 65$ Hz related to the electron percolation through mesoporous TiO_2 [15]. In the lowest frequency domain there is usually a third semicircle related to the ionic diffusion in the electrolyte [14] that we shall not analyze for the sake of simplification. An equivalent circuit already described in the experimental section action was used for fitting the data. Thus, symmetric cells were prepared and measured. Figure 3a shows the results relative to the photoelectrode–photoelectrode symmetric cell. The Nyquist plot shows three semicircles. In order of decreasing frequencies, they are: a first small semicircle, not very well defined, whose attribution to a certain physicochemical phenomenon is not unequivocal. We hypothesized an explanation related to the double optical fiber illumination mode, because the two-side photoelectrode illumination induced charge carrier dynamics in the TiO_2 layers closest to FTO, slightly different from TiO_2 bulk material. Although specific EIS studies on this aspect have not been done, Willig et al. [21] using photocurrent transient techniques described this situation. The second semicircle should be linked to the lifetime (τ_{eff}) of photoinjected electrons in the mesoporous material and the third one is related to the ionic diffusion, as it occurs in plain cells. Processing data with exclusion of very high and very low frequency points, we obtained values of τ_{eff} between 2.5 and 3 ms. These value is lower than ones found in literature [14], indicating a strong recombination process at the photoelectrode. This is a relevant clue that a low-quality TiO_2 film structure negatively affects the performance of our cells. Figure 3b shows the Nyquist plot of a counter–counter electrodes symmetric cell. Also in this plot we recognize a large dominating semicircle, but we now attribute this to charge transfer at the interface between Pt/FTO and electrolyte. Therefore, using the fitting procedure we have been able to evaluate the catalytic activity of the counterelectrode through calculation of R_{ct}, which is around 9.25 Ohm cm^2. At lower frequencies the feature of the ion diffusion through the electrolytic solution is present. As discussed before, it was decided not to fit the points of this frequency region. Anyway, in order to complete the cell analysis, we introduced the diffusion coefficient of I_3^- ($D_{I_3^-}$) in the electrolyte by using a different technique [4]. An extrapolated $D_{I_3^-}$ value of 6×10^{-6} cm^2 s^{-1} from slow scan cyclic voltammetry of the symmetric cell (not reported here) was taken. Table 1 summarizes the fitted parameters for both plain and

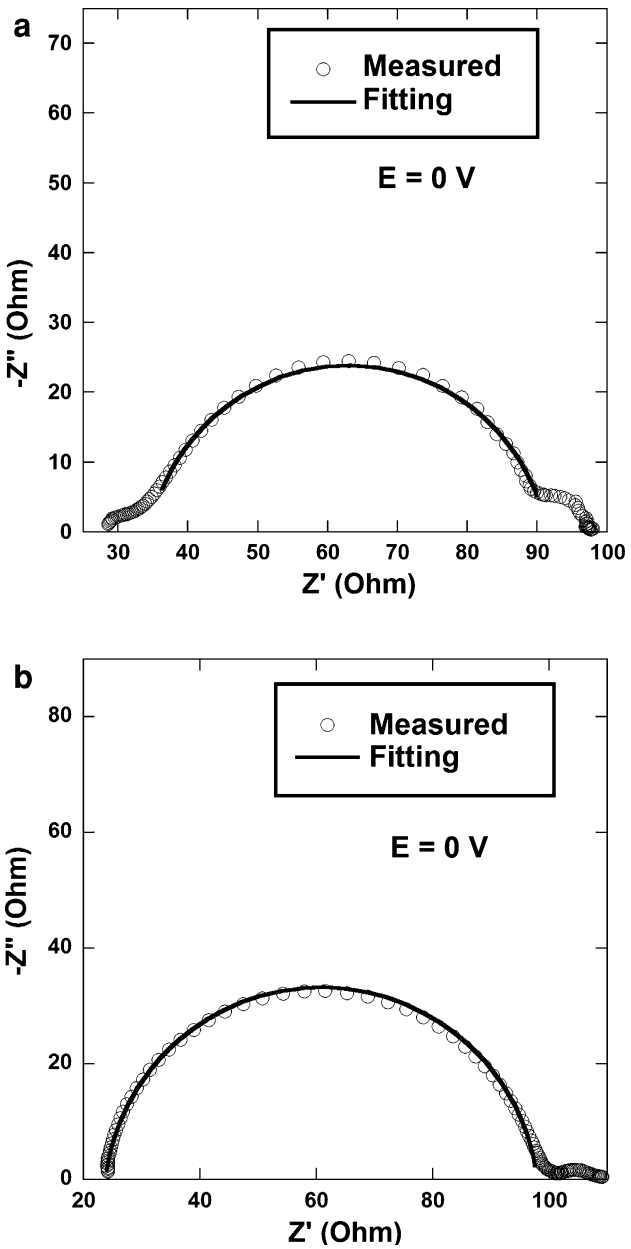

Fig. 3 **a** Nyquist plot of EIS spectra measured between 10^5 and 10^{-1} Hz on a photo–photo electrodes symmetric cell at cell voltage $E = 0$ V under illumination of 1,000 Wm^{-2}. (○) experimental data; (—) fitted data. **b** Nyquist plot of EIS spectra measured between 10^5 and 10^{-1} Hz on a counter–counter electrodes symmetric cell at cell voltage $E = 0$ V in dark condition. (○) experimental data; (—) fitted data

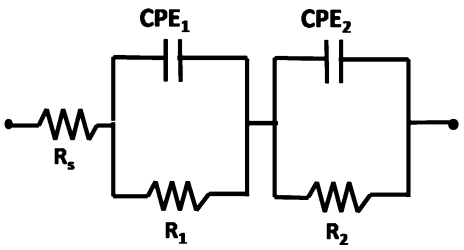

Fig. 4 Equivalent circuit proposed to fit the EIS data of plain and symmetric cells. In the latter case we assume $R_1 = R_2$ and $CPE_1 = CPE_2$

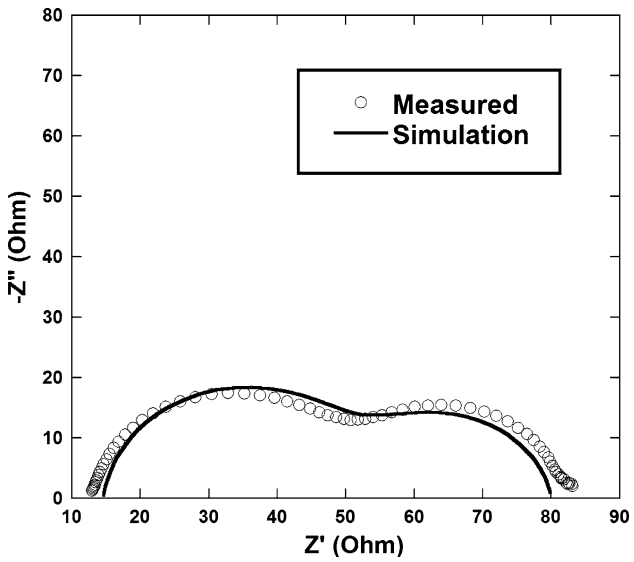

Fig. 5 Nyquist plot of data (—) generated by the simulation of a plain cell in comparison with experimental data (○)

symmetric cells; we underline that the values obtained with symmetric cells are in good agreement with ones of plain cells. Finally, in order to further confirm that this procedure can predict the behavior of the plain cell, a simulation was performed, assuming the equivalent circuit of Fig. 4 and taking as base parameters those calculated by fitting process. Figure 5 compares the Nyquist plot of the plain cell with the curve of the simulated one. The simulation reproduces quite well the trend of experimental data, with a natural mismatch due to the very simple model adopted. To the best of our knowledge, the symmetric cell technique has been used to study only the counterelectrode but has

Table 1 Plain and symmetric cell fitted parameters values

	R_s (Ω)	R_1 (Ω)	CPE_1 (Ss^n)	n_1	R_2	CPE_2 (Ss^n)	n_2
Plain cell	12.8	33.96	183.2	0.85	36.84	5.55	0.89
Photo–photo electrode	17.29	28.42	189.8	0.89	–	–	–
Counter–counter electrode	11.94	–	–	–	37.04	6.56	0.93

never been applied to photoelectrodes so far. The calculated data for both our counter and photoelectrode are comparable with literature data. The example shown in this paper gives a strong indication that our symmetric cell approach is self-consistent and permits the separate characterization of the photo and counterelectrode contributions in dye-sensitized solar cells.

4 Conclusion

The EIS technique is commonly used to characterize DSC devices, and the symmetrical cells approach can help in solving the issue of data analysis. So far, only counter–counter electrode cells have been studied, but in this work also photoelectrode–photoelectrode symmetric cells have been introduced. The data fitting on symmetric cells yielded parameter comparable to literature and consistent with the measurement of a complete cell. The latter has been confirmed by simulation process. This promising result opens the door to a more accurate investigation of the inner DSC phenomena, focusing attention separately on TiO_2/dye/electrolyte or electrolyte/Pt/TCO interfaces.

Acknowledgements Financial support from "Regione Lazio" is gratefully acknowledged. The authors wish to thank Dr. E. Petrolati for helping in data elaboration.

References

1. O'Regan B, Grätzel M (1991) Nature 353:737
2. Han L, Koide N, Chiba Y et al (2005) Appl Phys Lett 86:213501
3. Onoda K, Ngamsinlapasathian S et al (2007) Solar Energy Mat Solar Cells 91:1176
4. Hauch A, Georg A (2001) Electrochim Acta 46:3457
5. Ho Yoon C, Vittal R, Lee J et al (2008) Electrochim Acta 53:2890
6. Hoshikawa T, Ikebe T et al (2005) Electrochim Acta 51:5286
7. Kun Koo B, Yoon Lee D et al (2006) J Electroceram 17:79
8. Muratami T, Grätzel M (2008) Inorg Acta 361:572
9. Ponomarev E, Peter L (1995) J Electroanal Chem 396:219
10. Waita S, Aduda B et al (2007) J Electroanal Chem 605:151
11. Peter L, Poomarev E (1997) J Electroanal Chem 427:79
12. Huber R, Moser J, Grätzel M et al (2000) J Phys Chem B 104:8995
13. Hagfedt A, Lindquist S et al (1997) J Phys Chem B 101:2514
14. Wang Q, Moser J, Grätzel M (2005) J Phys Chem B 109:14945
15. Kern R, Sastrawan R et al (2002) Electrochim Acta 47:4213–4225
16. Han L, Koide N et al (2004) Appl Phys Lett 84:2433
17. Bisquert J, Grätzel M et al (2006) J Phys Chem B 110:11284
18. Bisquert J, Fabregat-Santiago F et al (2005) Solar Energy Mat Solar Cell 87:117
19. Cahen D, Hodes G, Grätzel M et al (2000) J Phys Chem B 104:2053
20. Wienke J, Kroon J et al (1997) ECN library Report rx97033
21. Willig F, Schwarburg K et al (2004) Coord Chem Rev 248:1259